AD-A113 038 PRINCETON UNIV NJ DEPT OF CHEMICAL ENGINEERING F/G 9/2
AUTOMATED TORSION PENDULUM: CONTROL AND DATA COLLECTION/REDUCTI--ETC(U)
APR 82 J B ENNS, J K GILLHAM N00014-76-C-0200
UNCLASSIFIED TR-24 NL

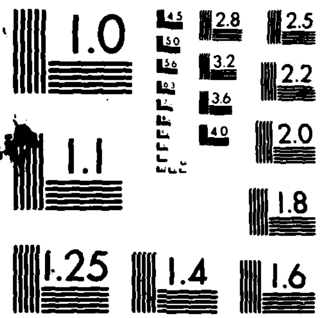

MICROCOPY RESOLUTION TEST CHART
NATIONAL BUREAU OF STANDARDS-1963-A

(12)

AD A113038

OFFICE OF NAVAL RESEARCH

Contract N00014-76-C-0200

Task No. NR 356-504

TECHNICAL REPORT NO. 24

AUTOMATED TORSION PENDULUM: CONTROL AND DATA COLLECTION/REDUCTION USING A DESKTOP COMPUTER

by

John B. Enns and John K. Gillham

for publication in the

"Computer Applications in Coatings and Plastics"

Symposium Series, American Chemical Society

Princeton University
Polymer Materials Program
Department of Chemical Engineering
Princeton, NJ 08544

April 1982

Principal Investigator
John K. Gillham
609/452-4694

82 04 05 110

SECURITY CLASSIFICATION OF THIS PAGE (When Data Entered)

REPORT DOCUMENTATION PAGE

READ INSTRUCTIONS BEFORE COMPLETING FORM

1. REPORT NUMBER: Technical Report #24	2. GOVT ACCESSION NO.: AD-A113 838	3. RECIPIENT'S CATALOG NUMBER
4. TITLE (and Subtitle): Automated Torsion Pendulum: Control and Data Collection/Reduction Using a Desktop Computer		5. TYPE OF REPORT & PERIOD COVERED: March 1980-March 1982
		6. PERFORMING ORG. REPORT NUMBER
7. AUTHOR(s): John B. Enns and John K. Gillham		8. CONTRACT OR GRANT NUMBER(s): N00014-76-C-0200
9. PERFORMING ORGANIZATION NAME AND ADDRESS: Polymer Materials Program, Department of Chemical Engineering, Princeton University, Princeton, NJ 08544		10. PROGRAM ELEMENT, PROJECT, TASK AREA & WORK UNIT NUMBERS: Task No. NR 356-504
11. CONTROLLING OFFICE NAME AND ADDRESS: Office of Naval Research, 800 North Quincy St., Arlington, VA 22217		12. REPORT DATE: April 1982
		13. NUMBER OF PAGES: 29
14. MONITORING AGENCY NAME & ADDRESS (if different from Controlling Office)		15. SECURITY CLASS. (of this report)
		15a. DECLASSIFICATION/DOWNGRADING SCHEDULE

16. DISTRIBUTION STATEMENT (of this Report)

Approved for Public Release; Distribution Unlimited.

17. DISTRIBUTION STATEMENT (of the abstract entered in Block 20, if different from Report)

18. SUPPLEMENTARY NOTES

19. KEY WORDS (Continue on reverse side if necessary and identify by block number)

Torsion Pendulum	Instrumental Control
Torsional Braid Analysis	Data Processing
Transitions	Desktop Computer

20. ABSTRACT (Continue on reverse side if necessary and identify by block number)

A torsion pendulum interfaced with a desktop computer form an automated instrument for dynamic mechanical characterization of polymeric materials. The computer controls the initiation of the oscillations, collects the digitized data and calculates the shear modulus and loss modulus from the damped oscillations, utilizing one of four methods of analysis: 1) fitting the data points about the maxima and minima to a quadratic equation to obtain their times and amplitudes, from which the frequency and logarithmic decrement can be calculated;

DD FORM 1 JAN 73 1473 EDITION OF 1 NOV 65 IS OBSOLETE
S/N 0102-LF-014-6601

SECURITY CLASSIFICATION OF THIS PAGE (When Data Entered)

2) fitting the data to a four-parameter equation of motion by a least squares technique; 3) fitting the data to a six-parameter solution to the equation of motion by a non-linear least squares technique; and 4) taking the Fourier transform of the data, which results in a maximum at the frequency of the oscillation whose amplitude is inversely proportional to the damping coefficient. The advantages and disadvantages of each method are discussed and the results of torsion pendulum and torsion braid analysis (TBA) experiments are compared.

AMERICAN CHEMICAL SOCIETY SYMPOSIUM SERIES
"Computer Applications in Coatings and Plastics"
in press.

AUTOMATED TORSION PENDULUM: CONTROL AND DATA COLLECTION/REDUCTION USING A DESKTOP COMPUTER

John B. Enns and John K. Gillham
Polymer Materials Program
Department of Chemical Engineering
Princeton University
Princeton, New Jersey 08544

A torsion pendulum interfaced with a desktop computer form an automated instrument for dynamic mechanical characterization of polymeric materials. The computer controls the initiation of the oscillations, collects the digitized data and calculates the shear modulus and loss modulus from the damped oscillations, utilizing one of four methods of analysis: 1) fitting the data points about the maxima and minima to a quadratic equation to obtain their times and amplitudes, from which the frequency and logarithmic decrement can be calculated; 2) fitting the data to a four-parameter equation of motion by a least squares technique; 3) fitting the data to a six-parameter solution to the equation of motion by a non-linear least squares technique; and 4) taking the Fourier transform of the data, which results in a maximum at the frequency of the oscillation whose amplitude is inversely proportional to the damping coefficient. The advantages and disadvantages of each method are discussed and the results of torsion pendulum and torsion braid analysis (TBA) experiments are compared.

The torsion pendulum has proven to be an important and versatile tool in the study of dynamic mechanical properties of materials. In our laboratory it has been applied primarily to polymers, although elsewhere it has been used with a wide variety of materials, ranging from liquids to metals and ceramics. The basis of its wide appeal lies in its fundamental simplicity: information about the complex modulus of the material under investigation is obtained by simply observing the decaying oscillations of the pendulum. After the pendulum is set in motion, it is permitted to oscillate freely at its resonant frequency while the amplitude of the oscillatory wave decays. In an unautomated system it is a relatively simple but tedious task to calculate the shear modulus and the loss modulus from the period of the oscillation, its logarithmic decrement and the geometric constants of the system. The independent variable in the investigation of dynamic mechanical properties of a material is often temperature, but it can also be time, as in the case of chemically reactive or physically aging systems.

A variation of the torsion pendulum, torsional braid analysis (TBA), utilizes a supported specimen so that the dynamic mechanical properties of a sample can be monitored in the liquid as well as the solid states (1, 2). An inert multifilamented glass braid is impregnated with the sample (usually in its liquid state or in solution). The observed dynamic mechanical properties are relative due to the composite nature and complex geometry of the specimen.

The purpose of this paper is to describe an automated torsion pendulum controlled by a desktop computer, to discuss four separate methods of data analysis, and to compare the results of a torsion pendulum experiment and a TBA experiment using the same epoxy resin.

Instrumentation

A schematic diagram of the torsion pendulum is shown in Figure 1. Free oscillations are initiated by an angular step-displacement of the upper member of the pendulum. The response of the lower member is a damped wave at the natural frequency of the system, and therefore is related to the physico-mechanical properties of the specimen.

The damped oscillations are converted to an electrical signal by a non-drag optical transducer: light is passed through a pair of polarizers, one of which serves as the inertial mass of the pendulum, to a photo-detector. The temperature, humidity and gas (usually helium) surrounding the specimen are closely controlled.

The torsion pendulum has been interfaced with a digital desktop computer (Hewlett Packard 9825B) shown in the system diagram Figure 2 (3). The motors which align the specimen and initiate the waves are under computer control via the scanner (HP 3495A) and relays. At present the direction of the temperature scan and the status of the experiment (whether to hold, reverse, or terminate) at either of the temperature limits set by the programmer (Eurotherm Corp.) are under computer control as well, but the rate of temperature change and the limits are not. The amplified thermocouple and wave signals are digitized by a high speed digital voltmeter (HP 3437A) whose scan rate is programmable, and the scanner supervises the I/O activity. The computer calculates the frequency and damping parameters from the raw data and plots the dynamic mechanical properties of the specimen as a function of temperature and/or time. A photograph of the equipment is shown in Figure 3. A commercial version of the automated torsion pendulum/torsion braid analyzer is available from Plastics Analysis Instruments, Inc., P.O. Box 408, Princeton, New Jersey.

For each damped wave the computer goes through a control sequence, schematically represented in Figure 4. Since the specimen may twist due to an uneven distribution of thermal stresses, the alignment motor rotates the pendulum through a gear train to the same reference position at the start of each control sequence. To initiate the oscillations, a second motor rotates the pendulum a specified angular displacement against the tension of a spring. The pendulum is held in this cocked position until oscillations set up by the alignment and cocking procedure have decayed, at which time the clutch is disengaged and the pendulum swings back so as to oscillate about the reference position. The data are then collected and reduced. The temperature (or time, for isothermal runs) is measured with the specimen in the cocked position and again after the data are collected. After plotting the reduced data, the oscillation is monitored until it decays to within specified limits and the cycle repeats.

The data obtained from the torsion pendulum can be displayed in various modes (4): the shear modulus G' is given by

$$G' = KI\left(\frac{2\pi}{P}\right)^2\left[1 + \left(\frac{\Delta}{2\pi}\right)^2\right] \qquad (1)$$

or by its approximation

$$G' \cong 4\pi^2 KI\left(\frac{1}{P}\right)^2 \qquad (2)$$

where P is the period, Δ is the logarithmic decrement and K is a geometric constant. In a TBA experiment, where K is unknown, the relative rigidity $[\propto(1/P)^2]$ is measured. Usually the logarithmic decrement term in equation (1) is negligible; only in the transition regions, where $\Delta > 0.6$, does it become greater than one percent. In Figure 5 both the shear modulus and its approximation are plotted (5, 6): the curves are indistinguishable except in the transition regions. The energy lost during the deformation can be displayed in a variety of ways (Figure 5): loss modulus

$$G'' = 4\pi KI\alpha/P, \qquad (3)$$

logarithmic decrement

$$\Delta \cong \pi\frac{G''}{G'} = \alpha P = \pi\tan\delta, \qquad (4)$$

and damping coefficient α. A shift is observed in the maximum by which the transition temperature is identified: for example, $T_g(G'') < T_g(\Delta) < T_g(\alpha)$ for a solid-to-rubber transition. (For a rubber-to-solid transition the shift occurs in the reverse order.)

Software

An efficient algorithm is required to monitor the oscillatory wave signal in real time. The flow chart is shown in Figure 6. The algorithm is used to monitor the wave while waiting for it to decay (Figure 4: prior to I and between IV and V), and to collect the data (Figure 4: VI) for subsequent analysis. The routine will provide the approximate location of the extrema (peaks) in real time at a scan rate of up to 75 points per second. If a scan rate faster than 75 points per second is required, the maxima and minima are located after the data have been collected and before initiation of the next wave.

In order to digitize the signal efficiently, the scan rate (digitization rate) S, must be chosen to match the characteristics of the oscillations. The optimum scan rate is a function of the period (P) of the oscillation, the number of data points (N) collected per wave, the time required for the oscillations to decay to a specified limit, and the method of analysis used. The scan rate corresponding to 40 points per cycle ($S = 40/P$) provides an adequate representation of the oscillations for most data reduction methods (see later). A rough estimate of the period is obtained from the first quarter cycle after initiation, and the scan rate is adjusted accordingly. To locate the peaks, an interval consisting of $1 + 4R$ (where R is a function of scan rate, usually equal to 4) data points moves along as the data are acquired, and the local maxima and minima are located by determining whether the center datum point of the interval is greater than (for a maximum) or less than (for a minimum) both the first and last data points of that interval. As soon as this set of criteria is met the center datum point is stored: the next peak is then sought. The reason for using more than three consecutive data points is to insure that a noisy signal does not simulate a maximum or minimum. This method, although quite crude, is much faster than one which involves taking a derivative of the data to locate the peaks. After all the data points have been collected, an approximate determination of the peaks is made by searching for the maximum or minimum among the data points within each of the intervals in which a maximum or minimum was detected.

Data Reduction. The oscillatory motion of a freely moving torsion pendulum has been described by an equation of motion (4):

$$I\, d^2\theta/dt^2 + \eta_{dyn}\, d\theta/dt + G_{dyn}\theta = 0 \qquad (5)$$

where I is the moment of inertia, η_{dyn} is the dynamic viscosity, G_{dyn} is the elastic shear modulus, θ is the angular deformation, and t is the time. The solution is a damped sine wave:

$$\theta = \theta_o \exp(-\alpha t)\cos(\omega t + \phi) \qquad (6)$$

where θ_0 is a constant; α is the damping coefficient,

$$\alpha = \eta_{dyn}/2I \; ; \tag{7}$$

ω is the natural angular frequency (radians/sec),

$$\omega = [(\frac{G_{dyn}}{I}) - (\frac{\eta_{dyn}}{2I})^2]^{\frac{1}{2}} \; ; \tag{8}$$

and ϕ is a phase angle. The shear modulus, G', and loss modulus, G", can be derived from information in the wave:

$$G' = KI(\omega^2 + \alpha^2) \tag{9}$$

and

$$G'' = 2KI\alpha\omega \tag{10}$$

where K is a geometric constant.

Peak Finding Method. Since the approximate location of the peaks has already been determined, the data points about each peak are fitted to a quadratic equation

$$\theta = a + bt + ct^2 \tag{11}$$

by a least squares method. The optimum number of data points to be used in fitting the quadratic equation to the data has been determined to be those in the interval $\pm\ 0.2\pi$ (7). Since the data were obtained at a scan rate such that 40 points per cycle were collected, the number of points used for fitting a quadratic is $(0.4\pi/2\pi)40 = 8$; because the calculations require an odd number of data points, 9 data points are used. Linear least squares fitting of the experimental data points to the quadratic equation requires minimization of the summation of residuals

$$Q = \sum_{i=1}^{n} (f_i - \theta_i)^2 \tag{12}$$

where

$$f_i = a + bt_i + ct_i^2 \tag{13}$$

and θ_i are experimentally observed data at times t_i. From the requirement that Q must be minimized,

$$\frac{\partial Q}{\partial A_k} = 2 \sum_{i=1}^{n} (f_i - \theta_i) (\frac{\partial f_i}{\partial A_k}) = 0 \quad (k = 1 \text{ to } 3) \tag{14}$$

where $A_1 = a$, $A_2 = b$, and $A_3 = c$;

this results in a set of three linear equations written in matrix form:

$$\begin{bmatrix} \sum_i 1 & \sum_i t_i & \sum_i t_i^2 \\ \sum_i t_i & \sum_i t_i^2 & \sum_i t_i^3 \\ \sum_i t_i^2 & \sum_i t_i^3 & \sum_i t_i^4 \end{bmatrix} \begin{bmatrix} A_1 \\ A_2 \\ A_3 \end{bmatrix} = \begin{bmatrix} \sum_i \theta_i \\ \sum_i t_i\theta_i \\ \sum_i t_i^2 \theta_i \end{bmatrix} \tag{15}$$

If the time-axis data are offset so that the central datum point is zero, the odd powered summations are identically equal to zero, thus simplifying the matrix. The solution to this set of equations provides the parameters of the quadratic equation. The best estimate of the peak position is obtained from the first derivative

$$\frac{d\theta}{dt} = b + 2ct = 0, \tag{16}$$

$$t_p = -\frac{b}{2c} \tag{17}$$

and

$$\theta_p = a + b(-\frac{b}{2c}) + c(-\frac{b}{2c})^2 = a - \frac{b^2}{4c} \quad . \tag{18}$$

This procedure is performed for the first minimum and the following maximum, as well as for the last pair (the selection of which depends on the damping), and the period is calculated by dividing the elapsed time between the maxima by the number of cycles. The logarithmic decrement is obtained from the relation

$$\Delta = (\frac{2}{i-1})\ln[(\frac{\theta_1-\theta_o}{\theta_i-\theta_{i-1}})] \qquad (i = 3, 5, 7 \ldots) \tag{19}$$

where θ_i is the amplitude of the ith extremum.

<u>Least Squares Method (8)</u>. A torsion pendulum specimen has a tendency to change its rotational orientation during the course of an experiment due to an uneven distribution of stresses caused by volume expansion and contraction. This results in a drift in the baseline of the wave signal which can be represented by

$$\theta = \theta_o \exp(-\alpha t)\cos(\omega t + \phi) + Bt + C \tag{20}$$

where B is the drift coefficient and C is the offset. The corresponding differential equation can be written as

$$\frac{d^2\theta}{dt^2} + 2\alpha\frac{d\theta}{dt} + (\alpha^2 + \omega^2)\theta - C(\alpha^2 + \omega^2) - 2\alpha B - B(\alpha^2+\omega^2)t = 0 \tag{21}$$

which may be simplified to

$$D = \frac{d^2\theta}{dt^2} + A_1\frac{d\theta}{dt} + A_2\theta + A_3 t + A_4 = 0. \tag{22}$$

A_k (k = 1 to 4) are the parameters fitted by a linear least squares analysis to determine

$$\alpha = \frac{A_1}{2}, \tag{23}$$

and

$$\omega = [A_2 - (\frac{A_1}{2})^2]^{\frac{1}{2}} = \frac{2\pi}{P} \quad . \tag{24}$$

The derivative values of θ at any point i are calculated numerically from a quadratic equation which uses five consecutive points to obtain the first and second derivatives:

$$\frac{d\theta_i}{dt} = \left(\frac{-2\theta_{i-2} - \theta_{i-1} + \theta_{i+1} + 2\theta_{i+2}}{10h}\right) \tag{25}$$

$$\frac{d^2\theta_i}{dt^2} = \left(\frac{2\theta_{i-2} - \theta_{i-1} - 2\theta_i - \theta_{i+1} + 2\theta_{i+2}}{7h^2}\right) \tag{26}$$

where h is the time interval between data points.

The linear least squares fitting of n experimental data points to the differential form of the equation of motion involves minimization of the summation

$$Q = \sum_{i=1}^{n}(f_i - D_i)^2 \tag{27}$$

where

$$f_i = \frac{d^2\theta_i}{dt_i^2} + A_1\frac{d\theta_i}{dt_i} + A_2\theta_i + A_3 t_i + A_4 \tag{28}$$

is calculated from experimental data and D_i is identically zero by definition. From the requirement that Q is minimized,

$$\frac{\partial Q}{\partial A_k} = 2\sum_{i=1}^{n} f_i\left(\frac{\partial f_i}{\partial A_k}\right) = 0 \qquad (k = 1 \text{ to } 4). \tag{29}$$

This set of linear equations can be written in matrix notation:

$$\begin{bmatrix} \sum_i \dot\theta_i^2 & \sum_i \dot\theta_i\theta_i & \sum_i \dot\theta_i t_i & \sum_i \dot\theta_i \\ \sum_i \dot\theta_i\theta_i & \sum_i \theta_i^2 & \sum_i \theta_i t_i & \sum_i \theta_i \\ \sum_i \dot\theta_i t_i & \sum_i \theta_i t_i & \sum_i t_i^2 & \sum_i t_i \\ \sum_i \dot\theta_i & \sum_i \theta_i & \sum_i t_i & \sum_i 1 \end{bmatrix} \begin{bmatrix} A_1 \\ A_2 \\ A_3 \\ A_4 \end{bmatrix} = \begin{bmatrix} -\sum_i \ddot\theta_i\dot\theta_i \\ -\sum_i \ddot\theta_i\theta_i \\ -\sum_i \ddot\theta_i t_i \\ -\sum_i \ddot\theta_i \end{bmatrix} \tag{30}$$

When this expression is solved for A_k, the values of α and ω are obtained (Equations 23 and 24).

Non-Linear Least Squares Method (9). Assuming that (from equation 20)

$$\theta = A_1\exp(-A_2t)\cos(A_3t + A_4) + A_5t + A_6 \tag{31}$$

where now $A_1 = \theta_o$, $A_2 = \alpha$, $A_3 = 2\pi/P$, $A_4 = \phi$, $A_5 = B$ and $A_6 = C$ is an adequate representation of the solution to the equation of motion of a torsion pendulum, the parameters A_k ($k = 1$ to 6) can be determined by fitting the data (θ_i, t_i; $i = 1$ to n) to the solution.

If the values of the parameters A_k were known, it would be possible to evaluate

$$f_i = A_1\exp(-A_2t_i)\cos(A_3t_i + A_4) + A_5t_i + A_6 \tag{32}$$

for each t_i to obtain a set of "true" residuals

$$r_i = f_i - \theta_i \qquad (i = 1 \text{ to } n). \tag{33}$$

A "true" residual would represent the difference between the actual function value at t_i and the empirical value θ_i. These "true" residuals cannot be calculated because the actual values of the parameters A_k are not known.

However, initial estimates of the parameters A_k° can be obtained from other methods, or a previous wave, and "computed" residuals can be calculated:

$$R_i = A_1^\circ\exp(-A_2^\circ t_i)\cos(A_3^\circ t_i + A_4^\circ) + A_5^\circ t_i + A_6^\circ - \theta_i \tag{34}$$

$$(i = 1 \text{ to } n)$$

Improved estimates of the parameters A_k can be obtained by a differential correction technique based on least squares, provided that the estimates A_k° are sufficiently close to the actual values of the parameters A_k to lead to convergence of the method. This differential correction technique can be derived by first expanding the function about A_k° using a linear Taylor series expansion of the form

$$f(t_i, A_1, A_2, \ldots, A_6) = f(t_i, A_1^\circ, A_2^\circ, \ldots, A_6^\circ)$$

$$+ \frac{\partial f}{\partial A_1}(A_1 - A_1^\circ) + \frac{\partial f}{\partial A_2}(A_2 - A_2^\circ) + \ldots + \frac{\partial f}{\partial A_6}(A_6 - A_6^\circ) \qquad (35)$$

so that a relation between the r_i and R_i can be obtained. This relation can be found by evaluating the equation at each value of t_i and subtracting θ_i from both sides of the equation. Using the definitions

$$\delta A_k = A_k - A_k^\circ \qquad (36)$$

and

$$\frac{\partial f_i}{\partial A_k} = \left.\frac{\partial f_i}{\partial A_k}\right|_{t = t_i,\ A_k = A_k^\circ}; \qquad (37)$$

the result can be written in the form

$$f(t_i, A_1, A_2, \ldots, A_6) - \theta_i = f(t_i, A_1^\circ, A_2^\circ, \ldots, A_6^\circ)$$

$$+ \left(\frac{\partial f_i}{\partial A_1}\right) \delta A_1 + \ldots + \left(\frac{\partial f_i}{\partial A_6}\right) \delta A_6 - \theta_i \quad (i = 1 \text{ to } n) \qquad (38)$$

The desired relation between the r_i and R_i can then be found by substituting the expressions for r_i and R_i:

$$r_i = R_i + \left(\frac{\partial f_i}{\partial A_1}\right)\delta A_1 + \ldots + \left(\frac{\partial f_i}{\partial A_6}\right)\delta A_6, \quad (i = 1 \text{ to } n). \qquad (39)$$

This relation can be used to compute, from A_k°, a set of parameters A_k that minimizes the sum of the squares of the "true" residuals r_i, i.e.,

$$Q = \sum_{i=1}^{n} r_i^2 = \sum_{i=1}^{n} \left[R_i + \left(\frac{\partial f_i}{\partial A_1}\right)\delta A_1 + \ldots + \left(\frac{\partial f_i}{\partial A_6}\right)\delta A_6\right]^2. \qquad (40)$$

The function Q has a minimum value when all of its partials with respect to the δA_k are simultaneously zero:

$$\frac{\partial Q}{\partial(\delta A_k)} = 2 \sum_{i=1}^{n} (\frac{\partial f_i}{\partial A_k})R_i + (\frac{\partial f_i}{\partial A_k})(\frac{\partial f_i}{\partial A_1})\delta A_1 + \ldots$$

$$+ (\frac{\partial f_i}{\partial A_k})(\frac{\partial f_i}{\partial A_6})\delta A_6 = 0 \quad (k = 1 \text{ to } 6). \tag{41}$$

Rearranging,

$$\delta A_1 \sum_{i=1}^{n} (\frac{\partial f_i}{\partial A_k})(\frac{\partial f_i}{\partial A_1}) + \ldots + \delta A_6 \sum_{i=1}^{n} (\frac{\partial f_i}{\partial A_k})(\frac{\partial f_i}{\partial A_6}) =$$

$$- \sum_{i=1}^{n} (\frac{\partial f_i}{\partial A_k})R_i \qquad (k = 1 \text{ to } 6) \tag{42}$$

Evaluating this equation for each k, and writing the result in matrix form, the normal equations are obtained:

$$\begin{bmatrix}
\sum (\frac{\partial f_i}{\partial A_1})^2 & \sum \frac{\partial f_i}{\partial A_1}\frac{\partial f_i}{\partial A_2} & \sum \frac{\partial f_i}{\partial A_1}\frac{\partial f_i}{\partial A_3} & \sum \frac{\partial f_i}{\partial A_1}\frac{\partial f_i}{\partial A_4} & \sum \frac{\partial f_i}{\partial A_1}\frac{\partial f_i}{\partial A_5} & \sum \frac{\partial f_i}{\partial A_1}\frac{\partial f_i}{\partial A_6} \\
\sum \frac{\partial f_i}{\partial A_2}\frac{\partial f_i}{\partial A_1} & \sum (\frac{\partial f_i}{\partial A_2})^2 & \sum \frac{\partial f_i}{\partial A_2}\frac{\partial f_i}{\partial A_3} & \sum \frac{\partial f_i}{\partial A_2}\frac{\partial f_i}{\partial A_4} & \sum \frac{\partial f_i}{\partial A_2}\frac{\partial f_i}{\partial A_5} & \sum \frac{\partial f_i}{\partial A_2}\frac{\partial f_i}{\partial A_6} \\
\sum \frac{\partial f_i}{\partial A_3}\frac{\partial f_i}{\partial A_1} & \sum \frac{\partial f_i}{\partial A_3}\frac{\partial f_i}{\partial A_2} & \sum (\frac{\partial f_i}{\partial A_3})^2 & \sum \frac{\partial f_i}{\partial A_3}\frac{\partial f_i}{\partial A_4} & \sum \frac{\partial f_i}{\partial A_3}\frac{\partial f_i}{\partial A_5} & \sum \frac{\partial f_i}{\partial A_3}\frac{\partial f_i}{\partial A_6} \\
\sum \frac{\partial f_i}{\partial A_4}\frac{\partial f_i}{\partial A_1} & \sum \frac{\partial f_i}{\partial A_4}\frac{\partial f_i}{\partial A_2} & \sum \frac{\partial f_i}{\partial A_4}\frac{\partial f_i}{\partial A_3} & \sum (\frac{\partial f_i}{\partial A_4})^2 & \sum \frac{\partial f_i}{\partial A_4}\frac{\partial f_i}{\partial A_5} & \sum \frac{\partial f_i}{\partial A_4}\frac{\partial f_i}{\partial A_6} \\
\sum \frac{\partial f_i}{\partial A_5}\frac{\partial f_i}{\partial A_1} & \sum \frac{\partial f_i}{\partial A_5}\frac{\partial f_i}{\partial A_2} & \sum \frac{\partial f_i}{\partial A_5}\frac{\partial f_i}{\partial A_3} & \sum \frac{\partial f_i}{\partial A_5}\frac{\partial f_i}{\partial A_4} & \sum (\frac{\partial f_i}{\partial A_5})^2 & \sum \frac{\partial f_i}{\partial A_5}\frac{\partial f_i}{\partial A_6} \\
\sum \frac{\partial f_i}{\partial A_6}\frac{\partial f_i}{\partial A_1} & \sum \frac{\partial f_i}{\partial A_6}\frac{\partial f_i}{\partial A_2} & \sum \frac{\partial f_i}{\partial A_6}\frac{\partial f_i}{\partial A_3} & \sum \frac{\partial f_i}{\partial A_6}\frac{\partial f_i}{\partial A_4} & \sum \frac{\partial f_i}{\partial A_6}\frac{\partial f_i}{\partial A_5} & \sum (\frac{\partial f_i}{\partial A_6})^2
\end{bmatrix}
\begin{bmatrix} \delta A_1 \\ \delta A_2 \\ \delta A_3 \\ \delta A_4 \\ \delta A_5 \\ \delta A_6 \end{bmatrix}
=
\begin{bmatrix} -\sum \frac{\partial f_i}{\partial A_1} R_i \\ -\sum \frac{\partial f_i}{\partial A_2} R_i \\ -\sum \frac{\partial f_i}{\partial A_3} R_i \\ -\sum \frac{\partial f_i}{\partial A_4} R_i \\ -\sum \frac{\partial f_i}{\partial A_5} R_i \\ -\sum \frac{\partial f_i}{\partial A_6} R_i \end{bmatrix} \tag{43}$$

where

$$\frac{\partial f_i}{\partial A_1} = \exp(-A_2 t_i)\cos(A_3 t_i + A_4), \tag{44}$$

$$\frac{\partial f_i}{\partial A_2} = -A_1 t_i \exp(-A_2 t_i)\cos(A_3 t_i + A_4), \tag{45}$$

$$\frac{\partial f_i}{\partial A_3} = -A_1 t_i \exp(-A_2 t_i)\sin(A_3 t_i + A_4), \tag{46}$$

$$\frac{\partial f_i}{\partial A_4} = -A_1 \exp(-A_2 t_i)\sin(A_3 t_i + A_4), \tag{47}$$

$$\frac{\partial f_i}{\partial A_5} = t_i, \tag{48}$$

$$\frac{\partial f_i}{\partial A_6} = 1. \tag{49}$$

The solution, δA_k, of this set of normal equations is a first-order approximation of the changes in $\overset{\circ}{A}_k$ required to obtain the parameters A_k. If any $|\delta A_k| > \varepsilon$ (error limit), $\overset{\circ}{A}_k$ is replaced by $\overset{\circ}{A}_k + \delta A_k$ and the entire differential-correction procedure is repeated using these new estimates.

Fourier Transform Method. Another method of data reduction is to take a fast Fourier transform (FFT) of the wave (10). As indicated in Figure 7, the Fourier transform of a damped sine wave with a single frequency is a single maximum in the frequency domain at the frequency of the oscillation. The amplitude (H) of the transformed data as a function of angular frequency (ω) is given by (11)

$$H = \frac{\theta_o \, [\alpha^2(\alpha^2+\omega^2+\omega_o^2)^2 + \omega^2(\alpha^2+\omega^2-\omega_o^2)^2]^{1/2}}{(\alpha^2+\omega_o^2-\omega^2)^2 + (2\alpha\omega)^2} \tag{50}$$

where θ_o is the initial amplitude, α is the damping coefficient, and ω_o is the natural angular frequency of the oscillation. The amplitude of the peak is given by

$$H_{max} = \left(\frac{\theta_o}{\alpha}\right) \left[\left(\frac{\alpha^2 + \omega_o^2}{\alpha^2 + 4\omega_o^2}\right)\right]^{1/2} \approx \frac{\theta_o}{2\alpha} \qquad (\alpha \ll \omega_o) \tag{51}$$

from which α, the damping coefficient, is obtained.

Discussion. The four methods of data reduction were used to analyze the raw data of the same TBA specimen during a slow (0.25°C/min) temperature scan (Figure 8). A comparison of the spectra indicates that they all gave similar results over the range of period (0.3 to 1.8 sec) and logarithmic decrement (0.01 to 1.08) encountered in the experiment. (The automated torsion pendulum has been used to reduce data with a range of 0.1 to 15 sec. for the period, and 0.001 to 4.0 for the logarithmic decrement). In Figure 8 there is no appreciable difference in the relative rigidity, but in the logarithmic decrement the non-linear least squares reduction method produces the smoothest results, followed by the peak-finding method. The linear least squares and Fourier transform methods have considerable scatter. The linear least squares method also results in a small systematic difference in the logarithmic decrement from the other three.

Although the peak-finding method is the simplest way of deriving the period and logarithmic decrement from the raw data, it has some limitations in that at least 2.25 cycles of oscillation are required in order to do the calculation. This is a problem when the system approaches critical damping conditions. It also is difficult to calculate the logarithmic decrement at very low damping (when the peak amplitude changes only slightly during the time data is collected) due to the resolution of the digitizing voltmeter. Of the four methods discussed, the peak finding method is the most sensitive to the scan rate, since the number of data points about each peak that are fitted to the three-parameter quadratic equation should be at least nine as discussed earlier. Therefore the scan rate, which depends on the estimate of the period, needs to be quite close to 40/P, where P is the actual period. Also, a systematic error is introduced when this method is used, because the position of the peaks is a function of the damping as well as the period. As can be seen in Figure 9, the peaks shift to shorter times as the damping increases.

The least squares fitting method overcomes limitations of the peak finding method, but introduces some errors of its own. It is not as sensitive to the scan rate, as long as $S >> 2/P$ (the Nyquist frequency), and its accuracy increases with increasing number of data points. It was found empirically (8) that the error was reduced if an integral number of cycles was used in the analysis. Some error is introduced due to the fact that first and second derivatives of the raw data have to be taken.

The use of the non-linear least squares method does not require any derivatives, but needs an initial estimation and takes more time to compute, since several iterations (usually 3 or 4) are necessary to reduce the difference between the estimated and calculated values of the damping coefficient to within 0.1%. But since this method only requires between 100 and 150 data points without a loss in accuracy compared to as many as 1000 for the peak-finding and least squares methods, the scan rate can be reduced as much as 90% and the time required for the calculations is reduced to the order of a minute.

The Fourier transform method requires a minimum of 1024 data points to provide enough resolution to calculate the damping coefficient. The FFT of 1024 data points takes approximately a minute with the HP 9825B computer, so this constitutes a practical limit in resolution due to computer memory size and time considerations. So as not to introduce error, the damped oscillations must not be truncated; therefore it is important to adjust the scan rate and the number of data points so that the entire wave is collected. The major problem with using the FFT method is the difficulty in obtaining accurate values of α; the curve is Laurentian, and hence its amplitude at the maximum is difficult to obtain. One way around this is to use a curve fitting procedure, but then there is no advantage in using this method. Some alternatives may be to use a larger and faster computer, or a dedicated microprocessor such as the spectrum analyzer (HP 3582A), which can compute the FFT in real time. A practical feature of the FFT is in the display of the transformed data; any non-homogeneity of the signal due to other modes of motion will appear as secondary peaks, and so this method serves as an excellent way to monitor the oscillations.

Although comparison of the four methods shows that the smoothest reduced data for the given experiment were obtained using the non-linear least squares method, the ultimate quality depends on the quality of the sensor signals of the experiment. Published superior TBA spectra obtained using the linear least squares method (8), and the peak-finding method using an analog computer (2), were presumably the consequence of a better basic experiment than the one used in this report to compare (as in Figure 8) the data reduction methods.

Calibration

A calibration wire whose shear modulus is known can be used to determine the moment of inertia of the pendulum assembly, so that quantitative measurements of the dynamic mechanical properties of specimens can be made. The shear modulus of the calibration wire is obtained by measuring the period of oscillation of a simple torsion pendulum consisting of an aluminum rod suspended by the wire. The moment of inertia of this system is given by

$$I = m\left(\frac{r^2}{3} + \frac{\ell^2}{12}\right) \qquad (52)$$

where m is the mass, r is the radius and ℓ is the length of the rod.

The shear modulus G' of a wire is given by

$$G' = \frac{8\pi L I}{R^4 P^2} \qquad (53)$$

where L is the length and R is the radius of the wire. With the calibration wire (whose shear modulus was determined to be 9.789 × 10^{11} dyne/cm^2) as a specimen in the automated torsion pendulum, the moment of inertia of the pendulum that was used routinely in the subsequent experiments was determined to be 138.7 g-cm^2. The shear modulus of a film of known dimensions can then be calculated from the period and logarithmic decrement using the equation (4):

$$G' = \frac{4\pi^2 IL}{NP^2}\left(1 + \frac{\Delta^2}{4\pi^2}\right) - \frac{mga^2}{12N} \tag{54}$$

where N is a form factor:

$$N = \frac{ab^3}{3}(1 - 0.63\ b/a), \tag{55}$$

a is the width, b is the thickness ($b < a/3$), L is the length, m is the mass supported by the specimen and g is the gravitational constant.

Comparison of Torsion Pendulum and TBA

A film of an amine-cured epoxy, Epon 828 (Shell)/PACM-20 (DuPont) with $T_{g\infty} = 166°C$, was cured by heating it to 250°C in a helium atmosphere. The dynamic mechanical spectrum of this film is shown in Figure 5. For comparison, the corresponding spectrum of a specimen consisting of a multifilamented glass braid impregnated with the uncured resin and cured in the TBA apparatus by heating it to 200°C under helium atmosphere is shown in Figure 10.

It has been reported (12) that the shear modulus as measured by the torsion pendulum and TBA should differ only by a multiplicative constant below Tg and the logarithmic decrement should be identical. Although the spectra of Epon 828/PACM-20 obtained by torsion pendulum and torsional braid analysis show transitions at the same temperature (glass transition at 166°C and a secondary sub-glass transition at -28°C), the results indicate that the actual modulus and logarithmic decrement cannot be compared quantitatively. In Figure 11 the relative rigidity (TBA) has been shifted vertically for comparison with the torsion pendulum data; a vertical shift on a logarithmic scale is equivalent to multiplying by a constant. It is evident by comparing the curves in Figure 11 that there is only a qualitative correlation between them.

Conclusions

The automation of the torsion pendulum utilizing a desktop computer eliminates the tedious data analysis previously associated with that technique. Any one of four data reduction methods can be used; the experimental conditions will determine which is the optimum one to employ. The torsion pendulum technique provides quantitative values of shear modulus and logarithmic decrement and in the torsion braid mode provides a qualitative analysis of materials, especially in the liquid-to-solid transition region. In addition to providing the capability of using any one of four data reduction techniques, the computer has the advantage of storing the data on magnetic tape, where it is available to be accessed for further computation or to be plotted in whatever mode is most suitable. Since the computer is easily programmable, the software can readily be adapted to consider other variables or to control the experiment in other ways.

Acknowledgment. This research was partially supported by the Office of Naval Research.

Literature Cited

1. Gillham, J. K. AIChE Journal, 1974, 20, 1066.
2. Gillham, J. K. "Torsional Braid Analysis (TBA) of Polymers", in Developments in Polymer Characterization-3, J. V. Dawkins, Ed., Applied Science Publishers: London, 1982. Ch. 5.
3. Enns, J. B.; Gillham, J. K.; Doyle, M. J. ACS Div. Organic Coatings and Plastics Chemistry, Preprints, 1980, 43, 669.
4. McCrum, N. G.; Read, B. E.; Williams, G. Anelastic and Dielectric Effects in Polymeric Solids, John Wiley and Sons, Ltd: London, 1967.
5. Enns, J. B.; Gillham, J. K.; Small, R. ACS Polymer Division, Preprints, 1981, 22, 123.
6. Enns, J. B. Ph.D. Thesis, Princeton University, 1982.
7. Solomon, James, "Development of a Data Reduction Scheme for Torsional Braid Analysis: Curve Fitting by Least Squares". Senior Thesis, Dept. of Chemical Engineering, Princeton University, Princeton, NJ, April 1976.
8. Gillham, J. K.; Stadnicki, S. J.; Hazony, Y. J. Appl. Polymer Sci., 1977, 21, 40.
9. McCalla, T. R. Introduction to Numerical Methods and Fortran Programming. John Wiley & Sons, Inc.: New York, 1967.
10. Ackroyd, M. H. Digital Filters. Butterworths: London, 1973.
11. Champeney, D. C. Fourier Transforms and Their Physical Applications. Academic Press: New York, 1973.
12. Hartman, B; Lee, G. F. J. Appl. Polymer Sci., 1977, 21, 1341.

Figure Captions

Figure 1. Automated torsion pendulum: schematic. An analog electrical signal is obtained from passing a light beam through a pair of polarizers, one of which oscillates with the pendulum. The pendulum is aligned for linear response and initiated by a computer that also processes the damped waves to provide the elastic modulus and mechanical damping data which are plotted on an XYY plotter versus temperature or time.

Figure 2. Automated torsion pendulum: system schematic for interfacing with a digital computer. The torsion pendulum has been interfaced with a digital desktop computer (HP-9825B). The motors which align the specimen and initiate the waves are under computer control. The wave and amplified analog thermocouple signals reach the computer digitized via a digital voltmeter (HP-3437A). The scanner (HP-3495A) supervises the I/O activity. Upon receiving the digitized raw data the computer calculates the frequency and damping parameters, and plots the dynamic mechanical properties of the specimen as a function of temperature and time.

Figure 3. Automated Torsion Pendulum: the pendulum is housed in the cabinet at the left; the oven is separated from the optical transducer by an insulated 3/4 inch

horizontal aluminum plate. The temperature controller, digital voltmeter,scanner, and computer are in the rack at the right. The atmosphere control panel and liquid nitrogen container are shown in the background. One of the authors (JBE) is seated at the console.

Figure 4. Automated torsion pendulum: control sequence. I) Previous wave decays, drift detected and correction begins. II) Reference level of polarizer pair reached. III) Wave initiating sequence begins. IV) Decay of transients. V) Free oscillations begin. VI) Data collected. VII) Control sequence repeated.

Figure 5. Dynamic mechanical spectrum (torsion pendulum) of a cured film of Epon 828/PACM-20. Both the shear modulus G' (□) and its approximation $\underset{\sim}{G}'$ (◇) are plotted on the upper curve; the lower three curves are loss modulus G" (o), logarithmic decrement Δ (*), and damping coefficient α (+).

Figure 6. Flow diagram of data collection/peak-finding algorithm.

Figure 7. Fourier Transform Method. The Fourier transform of an exponentially damped sine wave of period P and damping coefficient α is a single maximum at the oscillation frequency whose amplitude is inversely proportional to the damping coefficient.

Figure 8. Dynamic mechanical spectrum (TBA) of Epon 828/PACM-20 in which the relative rigidity and logarithmic decrement have been calculated by four methods: peak-finding [PKF (□)], linear least squares [LSQ (*) , non-linear least squares [NLSQ (+)], and fast Fourier transform [FFT (o)]. For clarity the LSQ, NLSQ and FFT data have been displaced vertically in equal increments from the PKF data.

Figure 9. Damped Sine Wave. Error in measuring period by peak-finding method: the peaks of an exponentially damped sine wave of single frequency (0.5 Hz) shift to shorter times with increasing damping coefficient (α values: — 0.05, -- 0.5, -.- 1.0, — -- — 1.5).

Figure 10. Dynamic mechanical spectrum (TBA) of a cured composite specimen (glass braid impregnated with Epon 828/PACM-20 resin).

Figure 11. A comparison of torsion pendulum data obtained using a film [G' (□), Δ (*)] and TBA data obtained using a supported specimen [relative rigidity (◊), Δ (o)].

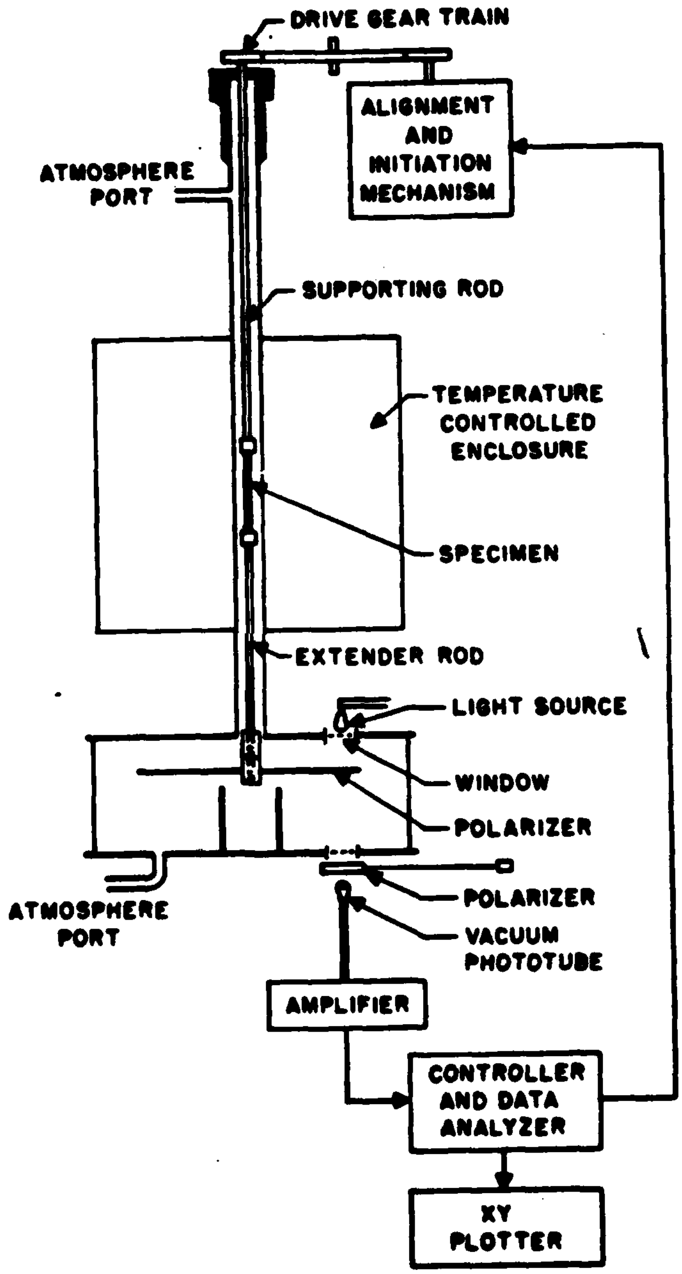
DRIVE GEAR TRAIN
ALIGNMENT AND INITIATION MECHANISM
ATMOSPHERE PORT
SUPPORTING ROD
TEMPERATURE CONTROLLED ENCLOSURE
SPECIMEN
EXTENDER ROD
LIGHT SOURCE
WINDOW
POLARIZER
ATMOSPHERE PORT
POLARIZER
VACUUM PHOTOTUBE
AMPLIFIER
CONTROLLER AND DATA ANALYZER
XY PLOTTER

Fig. 1

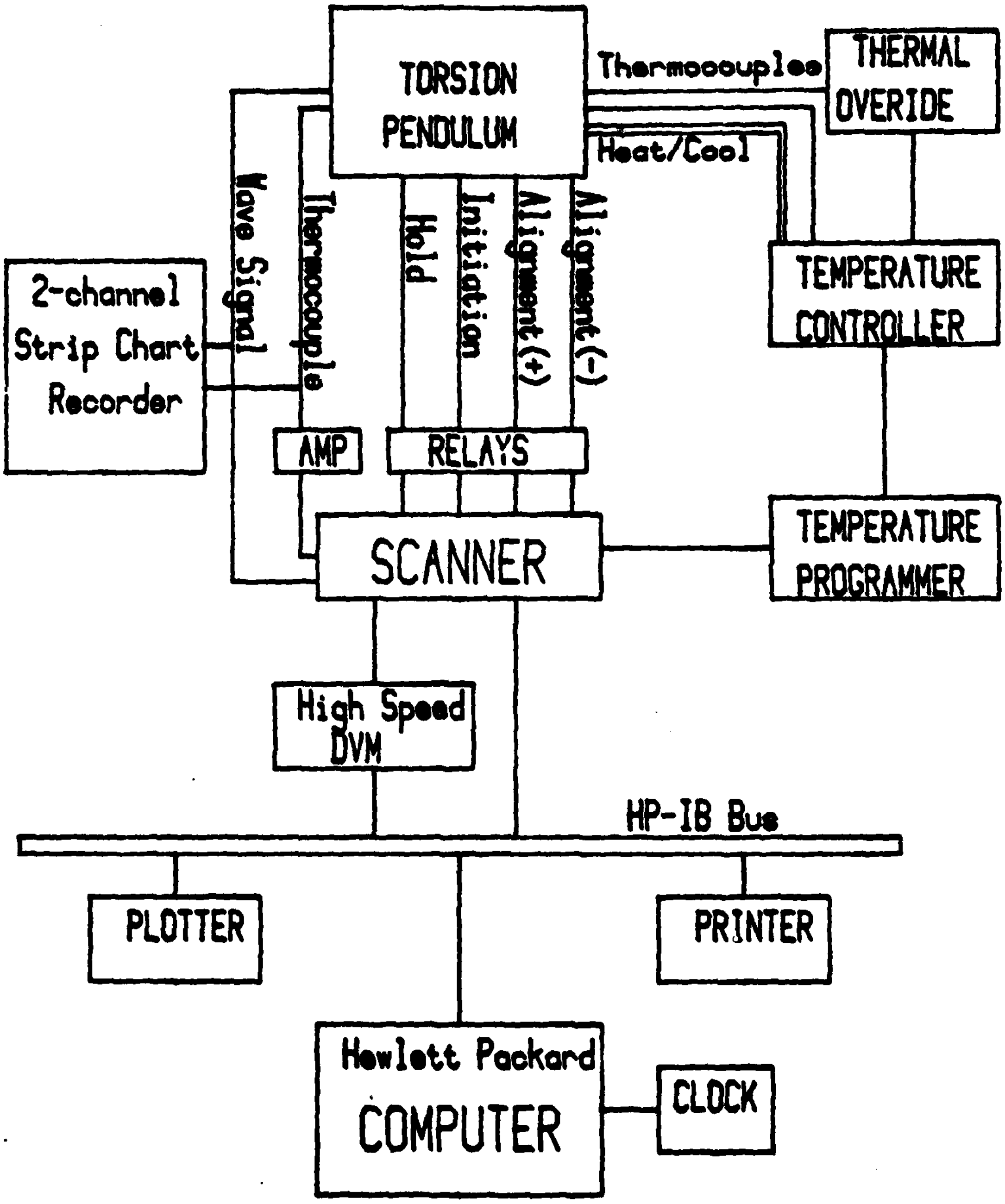
TORSION PENDULUM
Thermocouples
THERMAL OVERIDE
Heat/Cool
Wave Signal
Thermocouple
Hold
Initiation
Alignment (+)
Alignment (-)
2-channel Strip Chart Recorder
TEMPERATURE CONTROLLER
AMP
RELAYS
SCANNER
TEMPERATURE PROGRAMMER
High Speed DVM
HP-IB Bus
PLOTTER
PRINTER
Hewlett Packard COMPUTER
CLOCK

Fig. 2

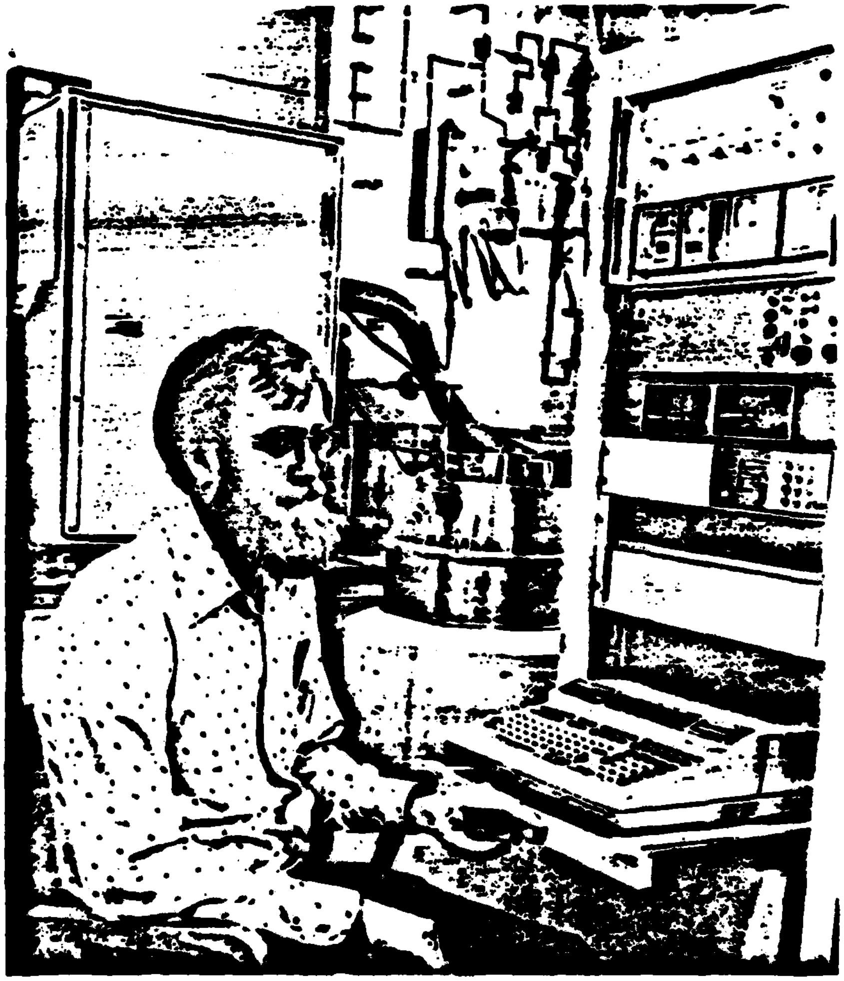

Fig. 3

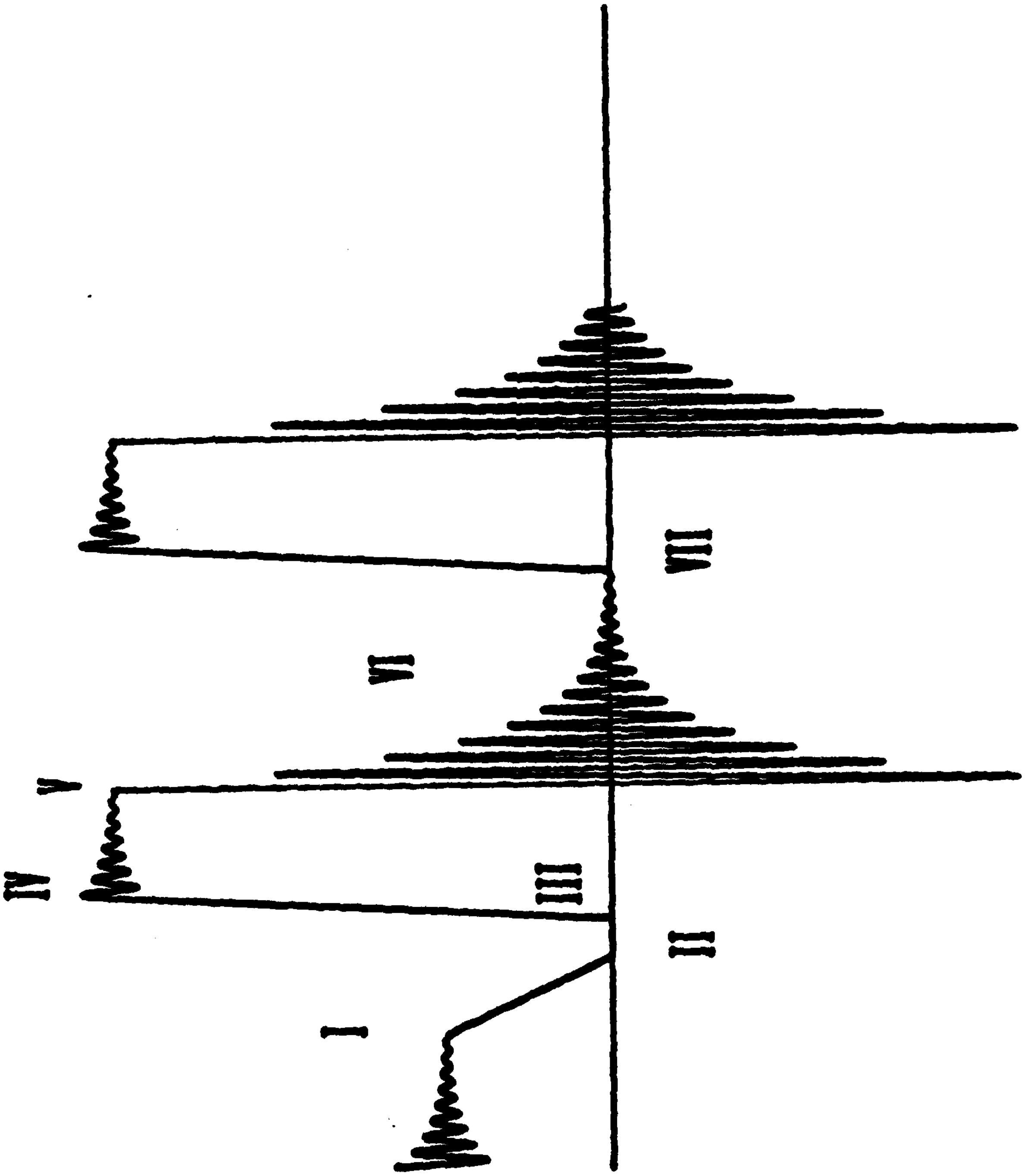

Fig. 4

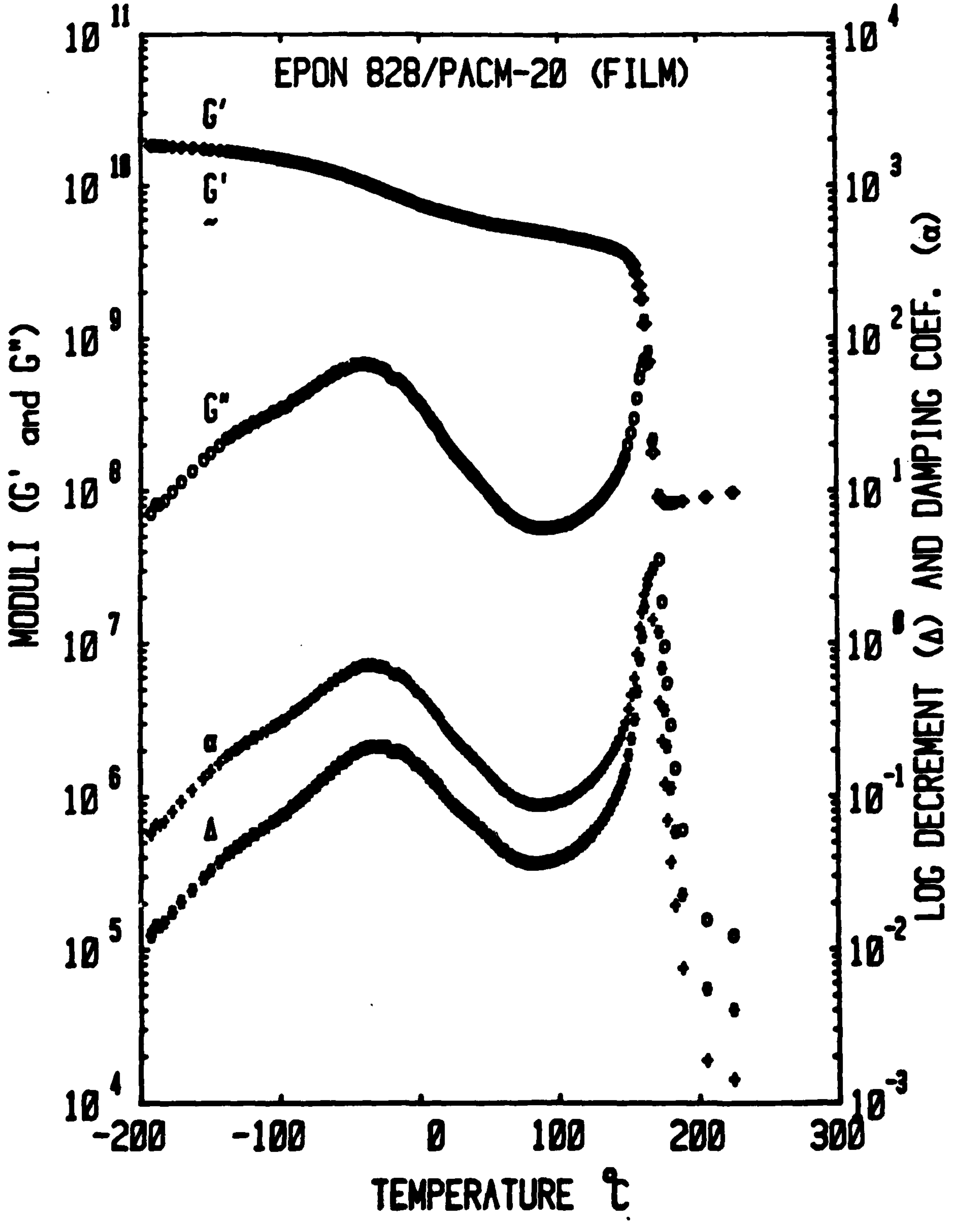
EPON 828/PACM-20 (FILM)
G'
G"
α
Δ
10^{11}
10^{10}
10^{9}
10^{8}
10^{7}
10^{6}
10^{5}
10^{4}
10^{4}
10^{3}
10^{2}
10^{1}
10^{0}
10^{-1}
10^{-2}
10^{-3}
-200
-100
0
100
200
300
MODULI (G' and G")
LOG DECREMENT (Δ) AND DAMPING COEF. (α)
TEMPERATURE ℃

Fig. 5

DATA COLLECTION

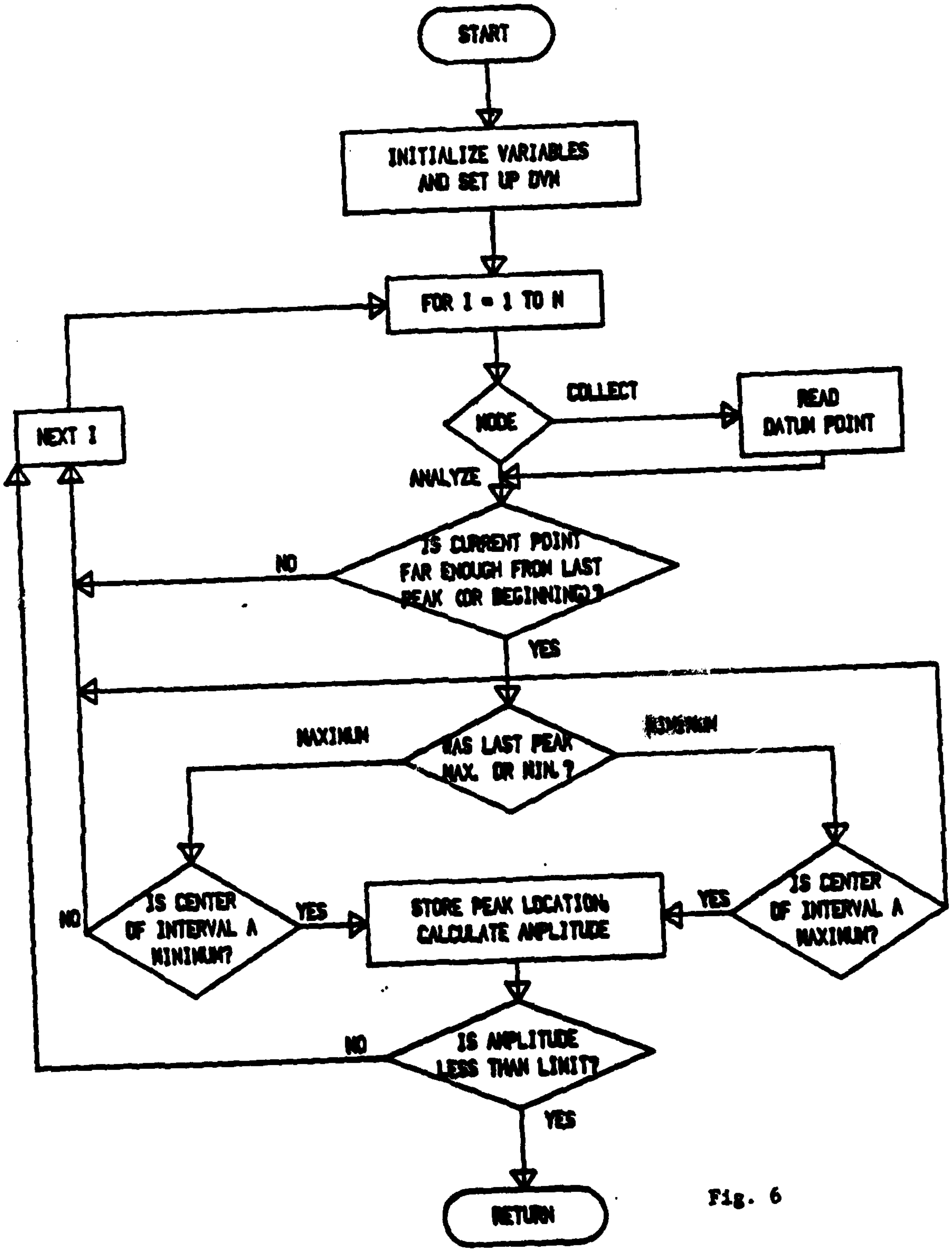

Fig. 6

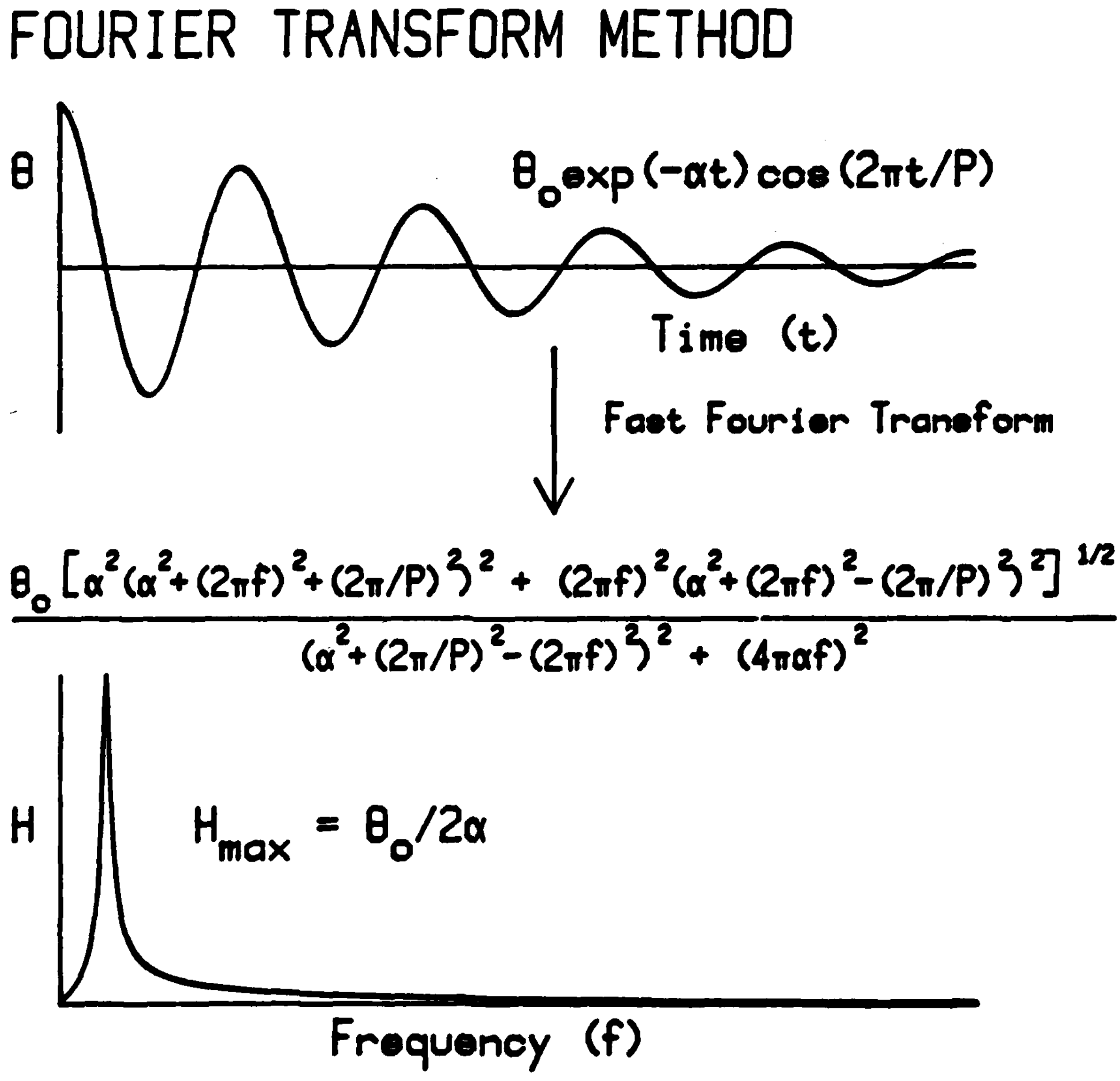
FOURIER TRANSFORM METHOD
θ
θo exp (-αt) cos (2πt/P)
Time (t)
Fast Fourier Transform
θo [α²(α²+(2πf)²+(2π/P)²)² + (2πf)²(α²+(2πf)²-(2π/P)²)²]^1/2 / (α²+(2π/P)²-(2πf)²)² + (4παf)²
H
Hmax = θo/2α
Frequency (f)

Fig. 7

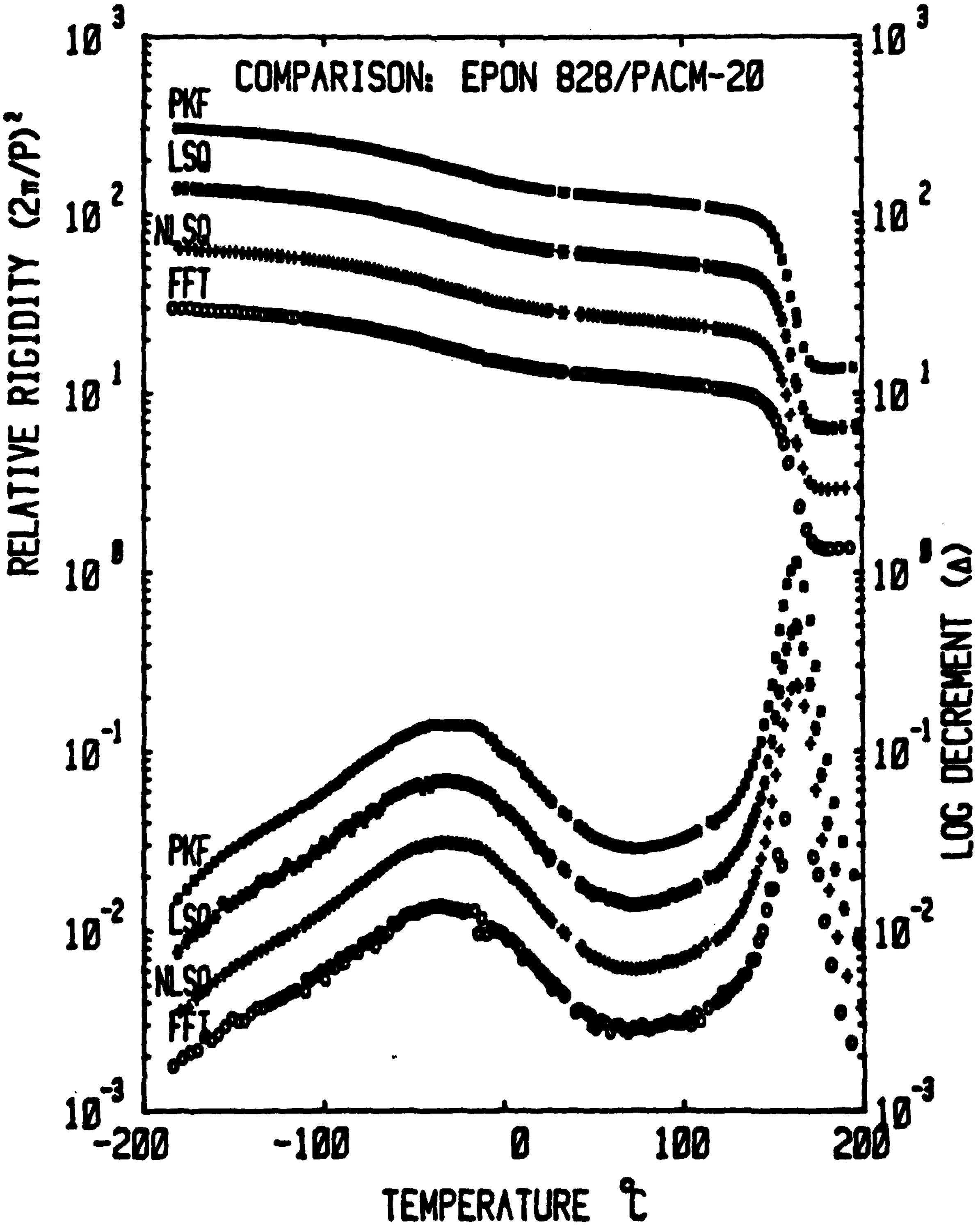
COMPARISON: EPON 828/PACM-20
PKF
LSQ
NLSQ
FFT
PKF
LSQ
NLSQ
FFT
RELATIVE RIGIDITY (2π/P)²
LOG DECREMENT (Δ)
TEMPERATURE ℃
10³
10²
10¹
10⁰
10⁻¹
10⁻²
10⁻³
-200
-100
0
100
200

Fig. 8

DAMPED SINE WAVE (TBA signal)

Eqn. of motion: $I \dfrac{d^2\theta}{dt^2} + n_{dyn} \dfrac{d\theta}{dt} + G_{dyn}\,\theta = 0$

Solution: $\theta = \theta_o \exp(-\alpha t)\cos(\omega t)$

Shear modulus: $G' = KI(\omega^2 + \alpha^2)$

Loss modulus: $G'' = KI\omega\alpha$

where $\omega = 2\pi/P$, $\alpha = \Delta/P$ and $\Delta = \ln(\Lambda_n/\Lambda_{n+1})$

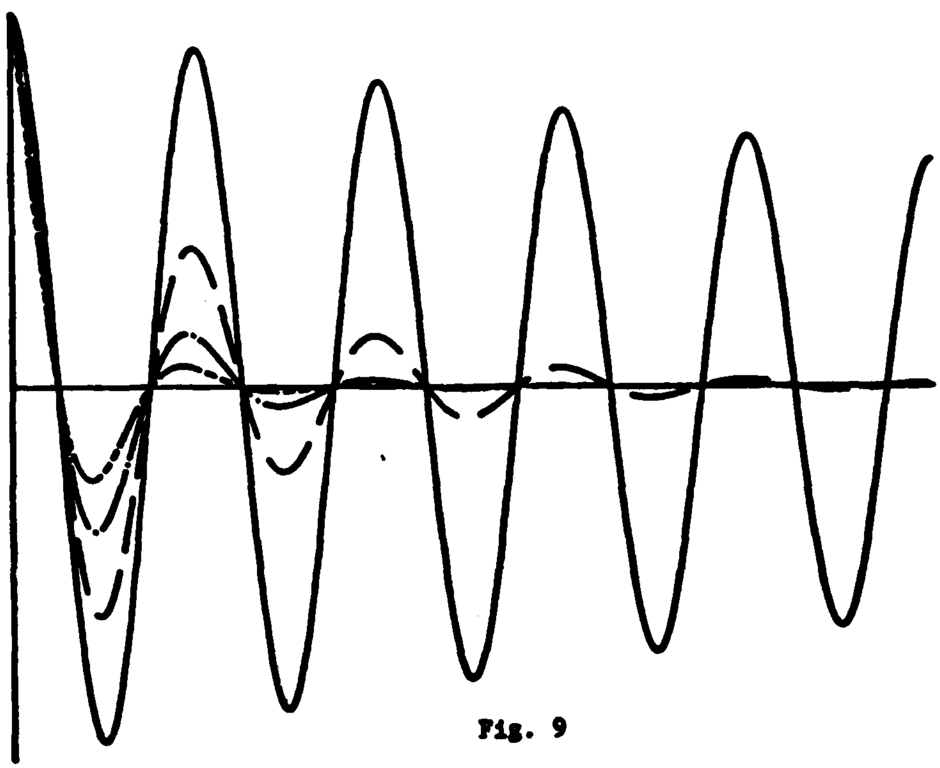

Fig. 9

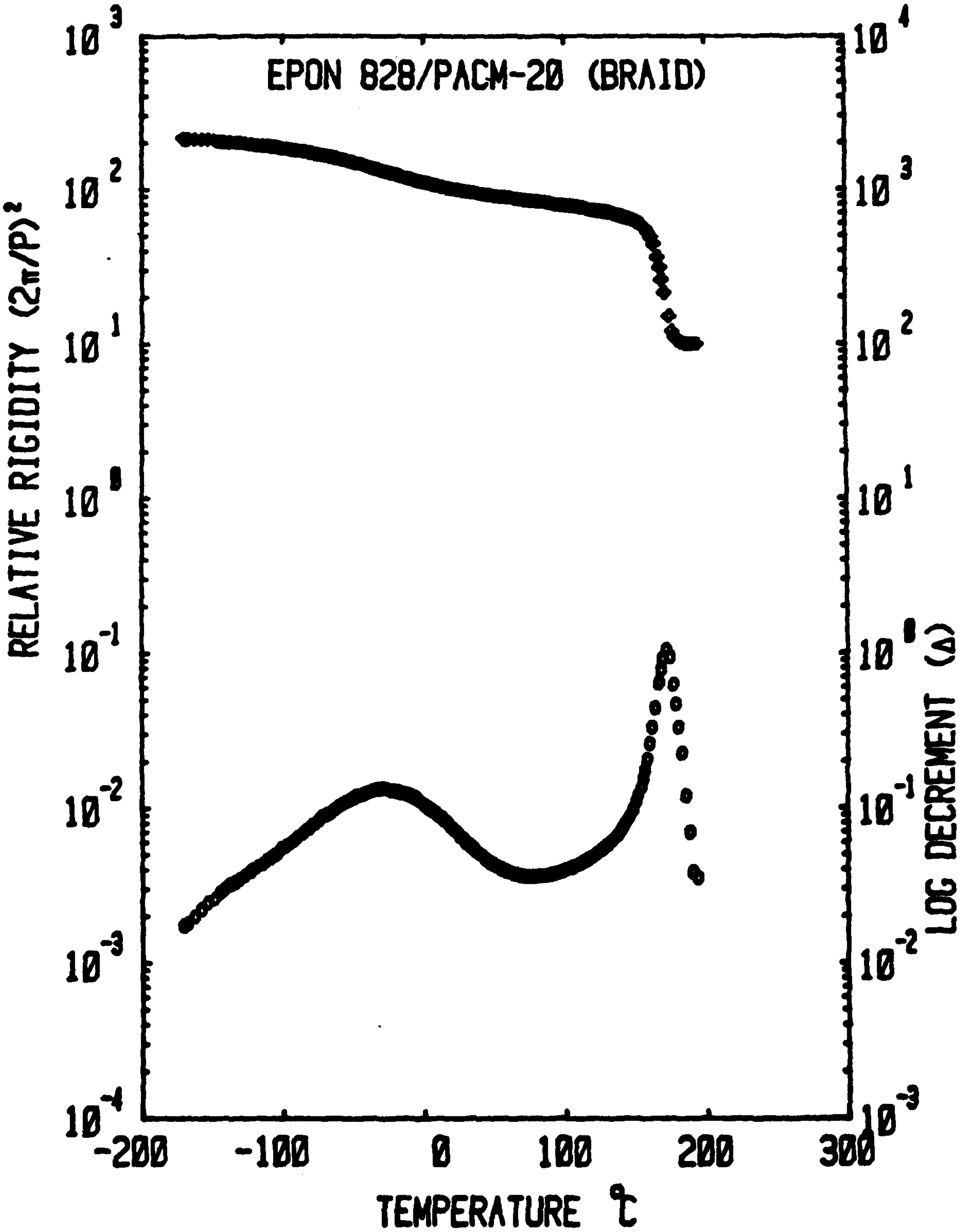
EPON 828/PACM-20 (BRAID)
RELATIVE RIGIDITY $(2\pi/P)^2$
LOG DECREMENT (Δ)
TEMPERATURE °C
10^3
10^2
10^1
10^0
10^{-1}
10^{-2}
10^{-3}
10^{-4}
10^4
10^3
10^2
10^1
10^0
10^{-1}
10^{-2}
10^{-3}
-200
-100
0
100
200
300

Fig. 10

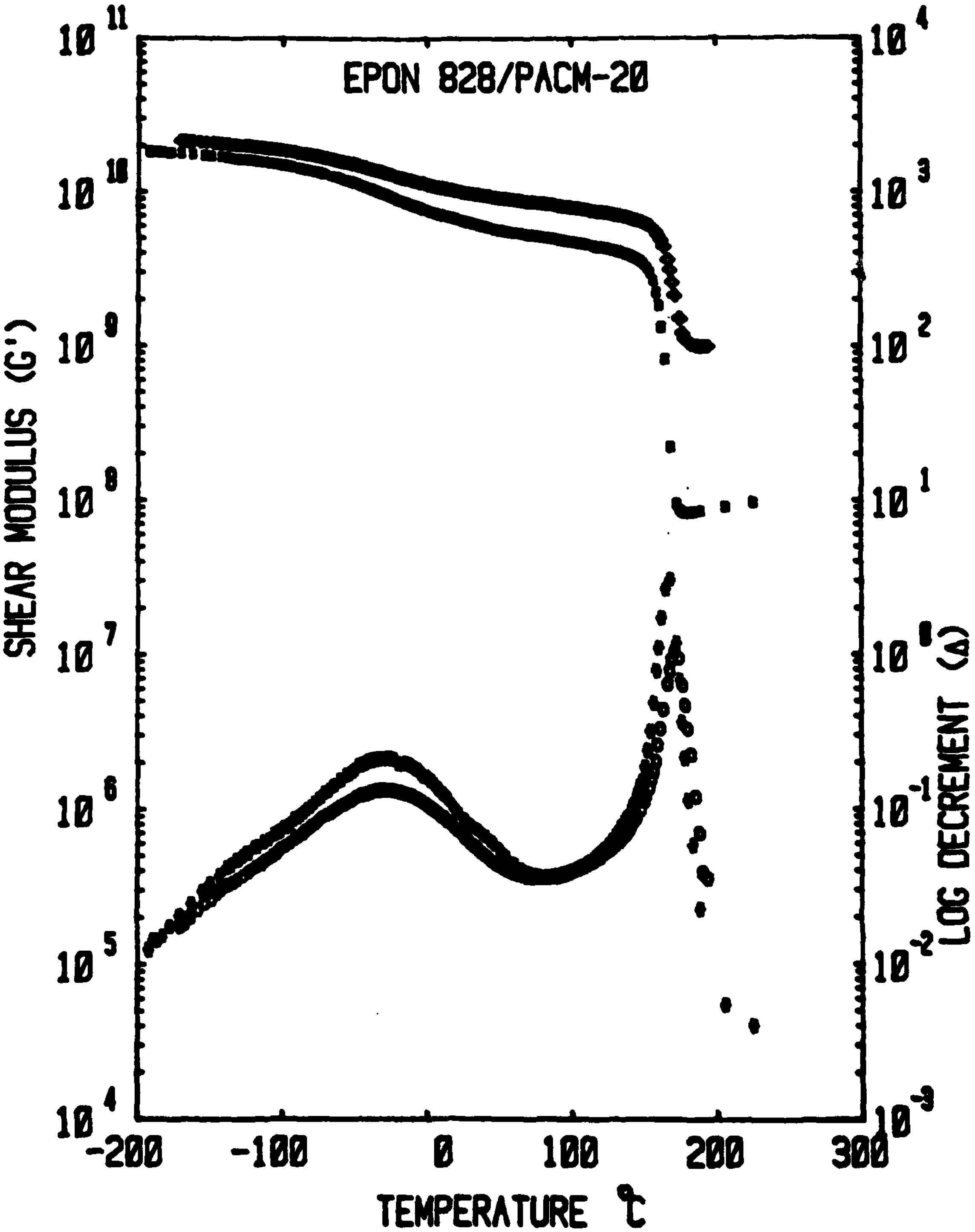
EPON 828/PACM-20
SHEAR MODULUS (G')
LOG DECREMENT (Δ)
TEMPERATURE °C
10 11
10 10
10 9
10 8
10 7
10 6
10 5
10 4
10 4
10 3
10 2
10 1
10 0
10 -1
10 -2
10 -3
-200
-100
0
100
200
300

Fig. 11

SP472-3/A1

472:GAN:716:enj
78u472-608

TECHNICAL REPORT DISTRIBUTION LIST, GEN

	No. Copies
Office of Naval Research Attn: Code 472 800 North Quincy Street Arlington, Virginia 22217	2
ONR Western Regional Office Attn: Dr. R. J. Marcus 1030 East Green Street Pasadena, California 91106	1
ONR Eastern Regional Office Attn: Dr. L. H. Peebles Building 114, Section D 666 Summer Street Boston, Massachusetts 02210	1
Director, Naval Research Laboratory Attn: Code 6100 Washington, D.C. 20390	1
The Assistant Secretary of the Navy (RE&S) Department of the Navy Room 4E736, Pentagon Washington, D.C. 20350	1
Commander, Naval Air Systems Command Attn: Code 310C (H. Rosenwasser) Department of the Navy Washington, D.C. 20360	1
Defense Technical Information Center Building 5, Cameron Station Alexandria, Virginia 22314	12
Dr. Fred Saalfeld Chemistry Division, Code 6100 Naval Research Laboratory Washington, D.C. 20375	1
U.S. Army Research Office Attn: CRD-AA-IP P.O. Box 1211 Research Triangle Park, N.C. 27709	1
Naval Ocean Systems Center Attn: Mr. Joe McCartney San Diego, California 92152	1
Naval Weapons Center Attn: Dr. A. B. Amster, Chemistry Division China Lake, California 93555	1
Naval Civil Engineering Laboratory Attn: Dr. R. W. Drisko Port Hueneme, California 93401	1
Department of Physics & Chemistry Naval Postgraduate School Monterey, California 93940	1
Scientific Advisor Commandant of the Marine Corps (Code RD-1) Washington, D.C. 20380	1
Naval Ship Research and Development Center Attn: Dr. G. Bosmajian, Applied Chemistry Division Annapolis, Maryland 21401	1
Naval Ocean Systems Center Attn: Dr. S. Yamamoto, Marine Sciences Division San Diego, California 91232	1
Mr. John Boyle Materials Branch Naval Ship Engineering Center Philadelphia, Pennsylvania 19112	1

TECHNICAL REPORT DISTRIBUTION LIST, GEN

	No. Copies
Mr. James Kelley DTNSRDC Code 2803 Annapolis, Maryland 21402	1
Mr. A. M. Anzalone Administrative Librarian PLASTEC/ARRADCOM Bldg 3401 Dover, New Jersey 07801	1

SP472-3/B5

472:GAN:716:enj
78u472-608

TECHNICAL REPORT DISTRIBUTION LIST, 356A

Address	No. Copies
Dr. Stephen H. Carr Department of Materials Science Northwestern University Evanston, Illinois 60201	1
Dr. M. Broadhurst Bulk Properties Section National Bureau of Standards U.S. Department of Commerce Washington, D.C. 20234	2
Professor G. Whitesides Department of Chemistry Massachusetts Institute of Technology Cambridge, Massachusetts 02139	1
Dr. D. R. Uhlmann Department of Metallurgy and Material Science Massachusetts Institute of Technology Cambridge, Massachusetts 02139	1
Naval Surface Weapons Center Attn: Dr. J. M. Augl, Dr. B. Hartman White Oak Silver Spring, Maryland 20910	1
Dr. G. Goodman Globe Union Incorporated 5757 North Green Bay Avenue Milwaukee, Wisconsin 53201	1
Professor Hatsuo Ishida Department of Macromolecular Science Case-Western Reserve University Cleveland, Ohio 44106	1
Dr. David Soong Department of Chemical Engineering University of California Berkeley, California 94720	1
Dr. Curtis W. Frank Department of Chemical Engineering Stanford University Stanford, California 94305	1
Picatinny Arsenal Attn: A. M. Anzalone, Building 3401 SMUPA-FR-M-D Dover, New Jersey 07801	1
Dr. J. K. Gillham Department of Chemistry Princeton University Princeton, New Jersey 08540	1
Dr. E. Baer Department of Macromolecular Science Case Western Reserve University Cleveland, Ohio 44106	1
Dr. K. D. Pae Department of Mechanics and Materials Science Rutgers University New Brunswick, New Jersey 08903	1
NASA-Lewis Research Center Attn: Dr. T. T. Serofini, MS-49-1 21000 Brookpark Road Cleveland, Ohio 44135	1
Dr. Charles H. Sherman Code TD 121 Naval Underwater Systems Center New London, Connecticut 06320	1
Dr. William Risen Department of Chemistry Brown University Providence, Rhode Island 02192	1
Dr. Alan Gent Department of Physics University of Akron Akron, Ohio 44304	1
Mr. Robert W. Jones Advanced Projects Manager Hughes Aircraft Company Mail Station D 132 Culver City, California 90230	1

SP472-3/B7

472:GAN:716:lab
78u472-608

TECHNICAL REPORT DISTRIBUTION LIST, 356A

	No. Copies
Dr. C. Giori IIT Research Institute 10 West 35 Street Chicago, Illinois 60616	1
Dr. R. S. Roe Department of of Materials Science and Metallurgical Engineering University of Cincinnati Cincinnati, Ohio 45221	1
Dr. Robert E. Cohen Chemical Engineering Department Massachusetts Institute of Technology Cambridge, Massachusetts 02139	1
Dr. T. P. Conlon, Jr., Code 3622 Sandia Laboratories Sandia Corporation Albuquerque, New Mexico	1
Dr. Martin Kaufmann, Head Materials Research Branch, Code 4542 Naval Weapons Center China Lake, California 93555	1
Professor S. Senturia Department of Electrical Engineering Massachusetts Institute of Technology Cambridge, Massachusetts 02139	1
Dr. T. J. Reinhart, Jr., Chief Composite and Fibrous Materials Branch Nonmetallic Materials Division Department of the Air Force Air Force Materials Laboratory (AFSC) Wright-Patterson AFB, Ohio 45433	1
Dr. J. Lando Department of Macromolecular Science Case Western Reserve University Cleveland, Ohio 44106	1
Dr. J. White Chemical and Metallurgical Engineering University of Tennessee Knoxville, Tennessee 37916	1

	No. Copies
Dr. J. A. Manson Materials Research Center Lehigh University Bethlehem, Pennsylvania 18015	1
Dr. R. F. Helmreich Contract RD&E Dow Chemical Co. Midland, Michigan 48640	1
Dr. R. S. Porter Department of Polymer Science and Engineering University of Massachusetts Amherst, Massachusetts 01002	1
Professor Garth Wilkes Department of Chemical Engineering Virginia Polytechnic Institute and State University Blacksburg, Virginia 24061	1
Dr. Kurt Baum Fluorochem Inc. 680 S. Ayon Avenue Azusa, California 91702	1
Professor C. S. Paik Sung Department of Materials Sciences and Engineering Room 8-109 Massachusetts Institute of Technology Cambridge, Massachusetts 02139	1
Professor Brian Newman Department of Mechanics and Materials Science Rutgers, The State University Piscataway, New Jersey 08854	1
Dr. John Lundberg School of Textile Engineering Georgia Institute of Technology Atlanta, Georgia 30332	1